The Effect of Sonication on the Dielectric Properties of Ceramics

V.M. Laletin, N.N. Poddubnaya*, V.V. Rubanik, P.A. Razbaev, M.V. Kudybin, V.K. Frolov and A.D. Shilin

Institute of Technical Acoustics of the National Academy of Sciences of Belarus, Vitebsk, Belarus

Abstract: The paper investigates the effect of high-power sonication on the dielectric properties of ceramics with a composition of 99.8 mol.% (90mol.% $BaTiO_3$ + 10mol.% $CaTiO_3$) and 0.2mol.% $NiFe_2O_4$. We obtained ceramics by conventional high-temperature processing using high-power sonication of varying duration at the milling stage. The structural, microstructural, and dielectric properties were investigated. It is shown that the high-power sonication at themilling stage improves the microstructure of the ceramics by reducing the grain size and increasing the density. This improves the dielectric properties of the ceramics: relative permittivity, dielectric loss tangent, Young's modulus, piezoelectric coefficient d_{31}, and the electromechanical coupling coefficient by up to 15%. At the same time, the sintering temperature of the ceramics decreases from 1380-1400°C to 1300°C.

Keywords: High-power sonication, Lead-free ceramic, Dielectric properties, Microstructure.

1. INTRODUCTION

Lead zirconate titanate-based materials exhibit excellent piezoelectric properties, making them popular in industrial applications. However, the environmental and health impacts of lead necessitate the search for safer alternative materials. For this reason, research into lead-free piezoelectric ceramics, such as bismuth sodium titanate, potassium sodium niobate, and barium titanate, has intensified in the last decade [1-11]. For example, [10] showed that doping with up to 0.25mol.% cobalt improves the piezoelectric properties of barium titanate. An improvement in the piezoelectric modulus of a composite consisting of 85mol.% $BaTiO_3$ + 15mol.% $CaTiO_3$ was reported in [11].

One of the methods for intensifying the sintering process at present is the ultrasonic activation of the batch before pressing and synthesis. As a result of repeated action of pulsed mechanical loads on the surface of the powder particles, accompanying the closure of cavitation bubbles and collisions of powder particles arising from their random movement under the action of ultrasound, the powder is dispersed. Due to the occurrence of a defective structure in the particles, powder activation is achieved, which allows us to talk about ultrasonic mechanical activation [12]. The aim of the presented work was to study the effect of high-power sonication on the dielectric properties of ceramics with the composition 99.8mol.% (90mol.% $BaTiO_3$ + 10mol.% $CaTiO_3$) and 0.2mol.% $NiFe_2O_4$. It is known that small additions of nickel ferrite to barium titanate intensify the sintering process [13]. Therefore, nickel ferrite was introduced into the mixture of barium titanate and calcium titanate powders.

*Address correspondence to this author at the Institute of Technical Acoustics of the National Academy of Sciences of Belarus, Vitebsk, Belarus;
E-mail: poddubnaya.n@rambler.ru

2. MATERIALS AND METHODS

2.1. Sample Preparation

To prepare the ceramics, we used synthesized nickel ferrite, barium titanate, and calcium titanate powders in the following ratio: 99.8mol% (90mol% $BaTiO_3$ + 10mol% $CaTiO_3$) and 0.2mol% $NiFe_2O_4$. Ethyl alcohol was added to the powder mixture and milled for 1 hour. The prepared batch was air-dried at room temperature. The batch was then divided into five equal-weight portions, four of which were sonicated at an oscillation frequency of 22 kHz and an amplitude of 20 μm with varying activation times and excess hydrostatic pressure (Table **1**) in an ethyl alcohol medium at a ratio of 10 g powder per 100 g alcohol.

The mixtures prepared under the specified conditions were dried at 30°C. The mixtures prepared under various conditions were pressed into briquettes under a pressure of $2x10^8$Pa, using an aqueous solution of polyvinyl alcohol as a plasticizer. The briquettes were sintered in air at temperatures of 1260, 1280, and 1300°C for two hours. The cooling rate of the ceramics in the furnace did not exceed 50°C/hour. The resulting ceramic blanks were subjected to plane-parallel grinding.

2.2. Research Methods

Grain size analysis of the powders was performed by laser diffraction in an ethanol medium using an ANALYSETTE 22 MicroTec plus. Two semiconductor lasers were used for particle size determination: one with green light (532 nm, 7 mW) for measuring small particles, and one with infrared light (850 nm, 9 mW) for measuring larger particles. The limits of permissible relative error in particle size measurements are 10%. Elemental analysis of the microstructure and chemical composition of the samples was performed using scanning electron microscopy (SEM). Elemental

Received on 01-06-2026 Accepted on 14-07-2026 Published on 18-07-2026

E-ISSN: 2410-4701/26

Table 1: Modes of high-powered sonication of mixtures of 99.8 mol.% $Ba_{0.9}Ca_{0.1}TiO_3$ + 0.2 mol.% $FeNi_2O_4$

Sonication mode	1	2	3	4	5
Sonication time t, min.	0	30	60	90	30
Excess hydrostatic pressure P, atm.	0	0	0	0	2

analysis data for different regions of the sample were averaged across the spectra. The phase composition of the samples was studied using X-ray diffraction analysis of the samples in *CuKα* radiation in the range 2θ = 20–80° at a scanning rate of 4°/min. Capacitance and dielectric loss tangent were measured with an E7-8 instrument at a frequency of 1 kHz. The permittivity was calculated using the formula:

$$\boldsymbol{\varepsilon} = C \cdot h/(\boldsymbol{\varepsilon}_o \cdot S),$$

where C is the capacitance, $\boldsymbol{\varepsilon}_o$ is the electric constant equal to $8.85 \cdot 10^{-12}$F/m; S is the electrode area, h is the sample thickness.

The resonance-antiresonance method was used to measure the piezoelectric modulus $\boldsymbol{d}_{31}$, the electromechanical coupling coefficient K_p, and Young's modulus ${}^{P}Y$. The values were calculated using the following formulas:

$$\boldsymbol{d}_{31} = \sqrt{8.3 \cdot 10^{-3} \cdot \frac{1}{\rho \cdot r^2} \cdot \frac{\Delta f}{f_p} \cdot \boldsymbol{\varepsilon}}$$

$$K_p = \frac{1}{\sqrt{1 + \frac{8}{\pi^2} \cdot \left(\frac{f_a^2}{f_{p1}^2} - 1\right)^{-1}}}$$

$${}^{P}Y = 9{,}5 \cdot f_p^2 \, r^2 \cdot \rho \cdot (1 - \sigma^2)$$

where ρ is the density of the sample, r is the radius of the sample (disk), f_p is the resonant frequency, f_a is the antiresonant frequency, $\Delta f = f_a - f_p$ is the difference between the antiresonant and resonant frequencies, $\boldsymbol{\varepsilon}$ is the permittivity, σ is Poisson's ratio.

The measurement error for the dielectric loss tangent is determined by the instrument's accuracy and is within 2%. Measurement errors for ceramic density do not exceed 5% and are determined by the accuracy of weight measurements and the linear dimensions of the samples. The measurement error for specific electrical permittivity, piezoelectric modulus, electromechanical coupling coefficient, and Young's modulus is calculated taking into account the measurement errors for capacitance, resonance frequencies, and the linear dimensions of the samples and is within 7%.

3. RESULTS AND DISCUSSION

Analysis of the average chemical element content values for the spectra of samples taken from different sites showed that the spread of the main elements does not exceed 1.5%, which is within the measurement error. Table **2** shows the spectra of a sample obtained without sonication and a sample after high-powered sonication (HPS) for 90 minutes.

Table **3** shows the maximum permittivity and Curie temperature values for ceramics obtained at different sintering temperatures. The temperature dependences of permittivity and dielectric loss tangent for ceramics

Table 2: Elemental Analysis of the Chemical Composition of Samples obtained under Different Sonication Modes

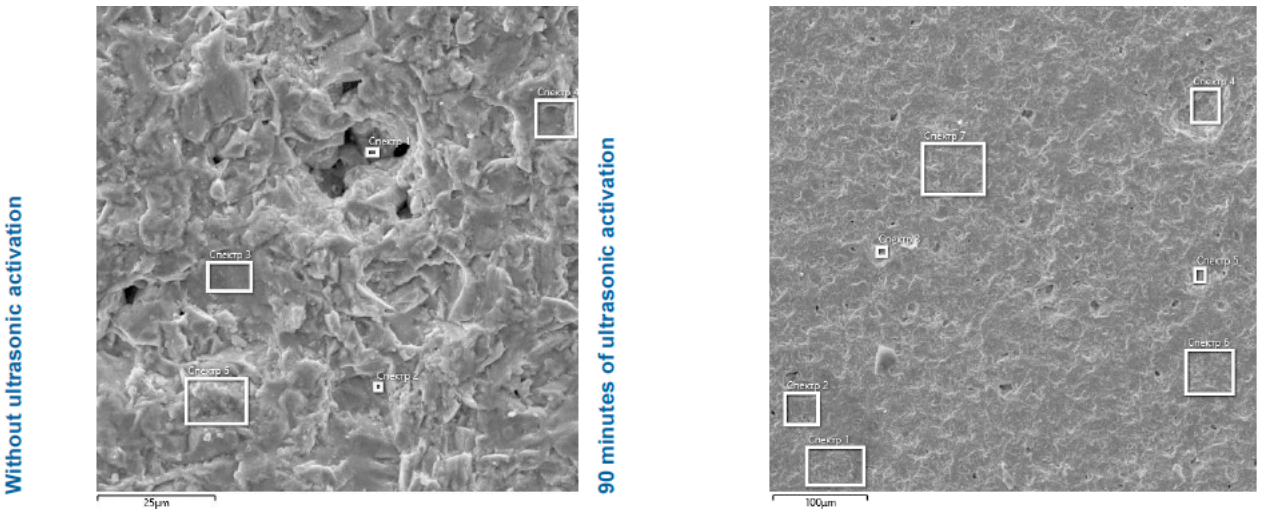

Spectrum	1	2	3	4	5	*Average*	Spectrum	1	2	3	4	5	6	7	*Average*
Fe	0,18	0,27	0,53	0,28	0,23	***0,30***	**Fe**	0,28	0,61	0,45	0,37	0,25	0,24	0,27	***0,35***
Ni	0	0,27	0	0	0	***0,05***	**Ni**	0,28	0	0	0	0	0	0,38	***0,09***
Ca	1,7	2	1,6	1,8	1,9	***1,80***	**Ca**	2	1,8	1,8	1,8	1,9	1,8	1,9	***1,9***
Ba	49,2	49	49,4	49,5	48,9	***49,20***	**Ba**	48,2	47,4	47,6	49,4	49,2	48,4	49,7	***48,6***
Ti	22,5	21,7	22,2	22	22	***22,08***	**Ti**	22,1	22,6	22,4	22,1	21,9	22,9	22,3	***22,3***
O	26,4	26,8	26,3	26,4	27,0	***26,6***	**O**	27,1	27,6	27,8	26,4	27,5	26,7	25,5	***26,9***

Table 3: Maximum Permittivity and Curie Temperature Values for Ceramics Obtained at Different Sintering Temperatures

Sintering temperatures	1260°C		1280°C		1300°C	
Modes	**T, °C**	**ε**	**T, °C**	**ε**	**T, °C**	**ε**
1	103	2961,4	101	6650,4	100	8128,9
2	116	1653,9	100	6857,3	100	8066,9
3	101	4340,7	102	6897,1	101	8281,0
4	101	5866,9	100	7760,1	99	8045,5
5	107	2920,0	100	5896,5	101	7733,0

obtained at different sintering temperatures are shown in Figure **1**.

The obtained results indicate that at ceramic sintering temperatures of 1280°C and 1300°C, the Curie temperature is approximately 101°C. In samples obtained from activated powders at 1280°C, an increase in permittivity is observed with increasing sonication – up to ~6860, 6900, and 7760 at 30, 60, and 90 minutes, respectively. Interestingly, a half-hour high-powered sonication using excess hydrostatic pressure leads to a decrease in permittivity to ~5900. In samples obtained at 1300°C, the maximum permittivity is observed in samples obtained from powders after an hour of sonication and is 8280, which is higher than the permittivity of samples from non-activated powders (8130). High-powered sonication in modes 2, 4, and 5 reduces the permittivity to 8070, 8045, and 7735. Thus, short-term and excessive exposure of powders to ultrasound leads to a decrease in permittivity. The excessive ultrasonic exposure allows obtaining powders with the smallest average grain size and additional internal energy, which likely results in a lower sintering temperature. Therefore sintering at elevated temperatures leads to cracking of the ceramics and a decrease in permittivity. Short-term exposure to ultrasound leads to a wide spread between the minimum and maximum grain sizes, sintered inhomogeneity, and deterioration of properties. The effect of high-powered sonication is most noticeable on ceramics obtained at a temperature of 1260°C. For samples obtained with sonication modes 3 and 4, the Curie temperature was 101°C, and for modes 1, 2 and 5 - 103°C, 116°C and 107°C, respectively. An increase in the Curie temperature generally indicates the presence of a two-phase system in which the reaction has not yet completed. The X-ray diffraction analysis is shown in Figure **2**. Due to the low ferrite concentration in the batch, we cannot confirm the presence and coexistence of two ceramic phases.

The dielectric constant of samples from unsonication powders was 2962, while for samples obtained after 30 minutes of high-powered sonication without excess hydrostatic pressure it was 1655, which is significantly lower. Sonication using excess hydrostatic pressure made it possible to return the dielectric constant of the samples obtained without ultrasonic activation. Sonication in modes 3 and 4 results in a single-phase mixture. The dielectric constant of the samples increases significantly, reaching 4340 after one hour and 5870 after one and a half hours of ultrasonic activation. Thus, 60 and 90 minutes of sonication lead to a complete reaction of the mixture, producing a single-phase solid solution already at 1260°C, which reduces the sintering temperature and increases the dielectric constant of the samples.

It is worth noting that the dielectric constant of the obtained samples without sonication is comparable to and higher than the data for the $Ba(Zr_{0.2}Ti_{0.8})O_3$-$x(Ba_{0.7}Ca_{0.3})TiO_3$ ceramics of similar

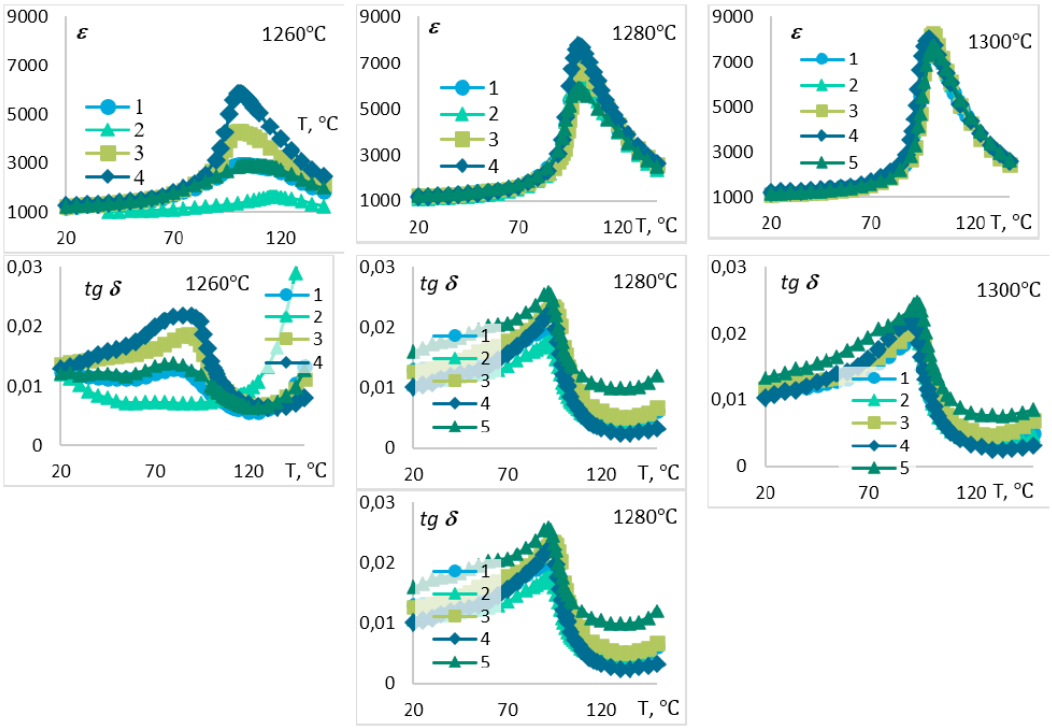

Figure 1: Temperature dependences of the permittivity and dielectric loss tangent of ceramics obtained at different sintering temperatures.

composition given in [11]. The phase transition temperature of 101°C is also 8°C higher than 93°C.

The behavior of the loss tangent correlates with the dependences of the relative permittivity. The tangent of samples sintered at a temperature of 1260°C undergoes the most significant changes. Thus, samples obtained in modes 1, 2, and 5, presumably retaining both phases, have minimal loss tangent values. Single-phase samples obtained from powders after high-powered sonication for 1 hour and 1.5 hours show higher loss tangent values, not exceeding 0.022. With an increase in sintering temperature to 1280°C, the effect of sonication has a less significant impact on the permittivity tangent, resulting in a change in the range of 0.0176 to 0.0258.

A colossal increase in the permittivity of barium titanate ceramics was achieved by the authors of [14]. In this case, it is associated with the substitution of barium with neodymium. In [15], it was shown that La substitution for Ba ions in the lattice leads to changes in

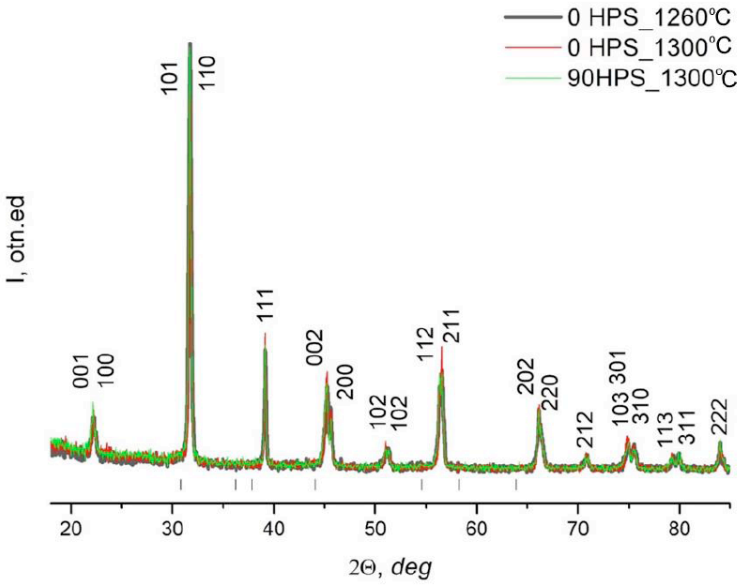

Figure 2: X-ray diffraction (XRD) spectra for ceramics. Experimental data are represented by solid lines of different colors. The vertical marks below the spectra correspond to experimental $NiFe_2O_4$ lines from the database.

the internal fields, the dynamics of phase transitions, and the conductivity of the samples. High-dielectric-constant $BaTiO_3$ ceramics were produced from $BaTiO_3$ and SiO_2 using ball milling and flash sintering. In this case, the increase in dielectric constant is due to the BST ($Ba_2TiSi_2O_8$, fresnoite) interface formed during sintering, which acts as an oxidation barrier during annealing and as a dielectric barrier in the final ceramic [16]. A detailed analysis of the effects of ultrasound on the structural, microstructural, dielectric, ferroelectric, and piezoelectric properties of $(Bi_{0.5}Na_{0.5})_{1-x}Ba_xTiO_3$ ceramics was conducted in [17]. Changes in the phase composition of the ceramics, lattice parameters, and changes in the size and shape of grains in ultrasonically treated samples were demonstrated. Similar changes in the dielectric characteristics of the ceramics were observed.

Maximum tangent values increase slightly with increasing sintering temperature and duration of sonication. In all cases, the loss tangent does not exceed 0.02 in the temperature range of 20–70°C. To explain the nature of the observed dependences, we first turn to the density values of the ceramic samples (Figure **3**).

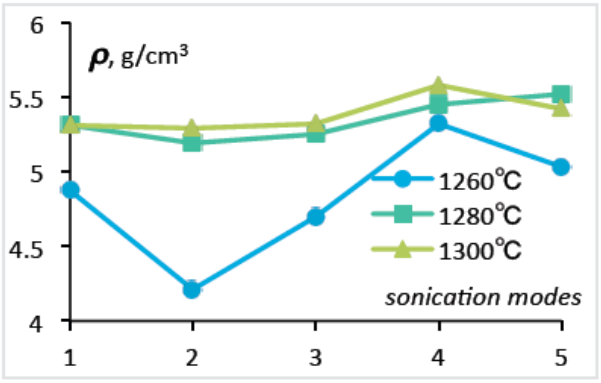

Figure 3: Dependence of ceramic density on high-powered sonication modes.

Clearly, samples obtained without ultrasonic activation at 1260°C have a low density (4.87 g/cm^3), indicating insufficient sintering temperature. Sonication leads to a significant decrease in sintered density after 30 minutes (to 4.21 g/cm^3) and an insignificant decrease (4.7 g/cm^3) after 60 minutes of exposure. Using excess hydrostatic pressure during high-powder activation allows for an increase in density to that of materials obtained without ultrasonic after just 30 minutes of exposure (5.03 g/cm^3). A similar, but less pronounced, pattern of density behavior can be observed at sintering temperatures of 1280°C and 1300°C. Sonication for 30 minutes reduces the sinter density (from 5.31 and 5.31 to 5.19 and 5.29 g/cm^3 for 1280°C and 1300°C), 60 minutes slightly returns the density to the initial values (5.25 and 5.32 g/cm^3, respectively), and after 90 minutes the density increases compared to the initial value (5.45 and 5.58 g/cm^3). Excessive hydrostatic exposure after just 30 minutes of sonication leads to an increase in the density of the ceramics (5.42 and 5.52 g/cm^3).

This behavior is caused by changes in grain size during sonication [12-13, 17-18]. With increasing duration of ultrasonic activation of the batch, the volume of fine powder fraction increases and reaches a maximum after 90 minutes of exposure. At the same time, the proportion of large particles will decrease with the duration of ultrasonic exposure. Moreover, the shorter the sonication duration, the greater the spread of grain sizes. A decrease in the average particle size in the batch and activation of the batch itself will lead to a slight decrease in the sintering temperature of the ceramics and an increase in the sintered density. In the work [19] the influence of the initial grain size of lead-free ceramic precursor powders $(Bi_{0.5}Na_{0.5})_{0.94}Ba_{0.06}TiO_3$ and the annealing temperature on the microstructure, dielectric and ferroelectric properties of ceramics was investigated. The initial powders were obtained by mixing the powders with an average grain size of 0.26 μm and 73 nm in different mass ratios (1:0, 1:1, 1:2 and 1:4). It is shown that at ratios of 1:2 and 1:4, ceramics annealed at 950°C exhibit dielectric and ferroelectric properties similar to those of BN6BT ceramics sintered at 1170°C by solid-phase sintering. In the article [20], a systematic investigation was conducted on the densification and grain growth of 170 and 260 nm tetragonal $BaTiO_3$ powders during high-temperature sintering. The activation energy for densification was shown to be lower for smaller particle sizes. This is explained by the higher surface energy per unit weight of small particles compared to large ones, which leads to a decrease in the energy barrier for compaction at any given sintering temperature and causes a decrease in the sintering temperature with a decrease in the grain size of the charge. Thus, the greater the proportion of large particles retained in the workpiece, the less uniform the sintering of the ceramics will be and the greater the size and number of pores in the finished ceramics. An increase in the duration of sonication exposure leads to an increase in the density of the finished ceramics due to grinding and activation of the batch. The presence of a large size in batch leads to pore formation, and the pore size decreases with increasing uniformity of grain sizes in the batch. With increasing density, the dielectric constant of the samples will also increase. The dielectric loss tangent is largely determined by the quality of the workpiece and will be significantly affected by the porosity of the samples and the homogeneity of the sintered product. Hydrostatic pressure increases the rate of particle size reduction, resulting in a minimum grain size. However, a sintering temperature of 1280°C will be too high for ceramics.

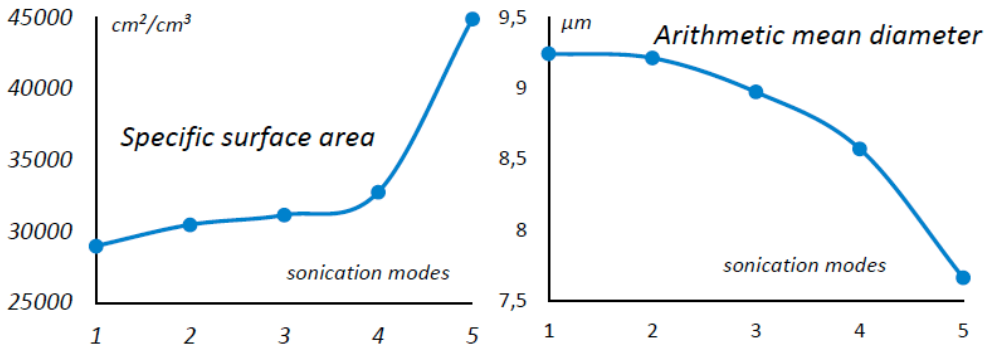

Figure 4: Results of particle size analysis of powders obtained under different sonication modes.

Despite the increased density, pores will remain in the sintered product, which correlates with an increase in the dielectric constant and permittivity values. The results of the powder particle size analysis are shown in Figure **4**.

Analysis of the above data shows that ceramics sintered at 1300°C exhibit the best dielectric properties. For these samples, the influence of sonication modes on the relative permittivity, dielectric loss tangent, Young's modulus, piezoelectric coefficient d_{31}, and electromechanical coupling coefficient was studied (Figure **5**, ***a***-***e***).

As mentioned earlier, increasing the ultrasonic exposure time from 30 to 90 minutes leads to an increase in the density and a decrease in the sintering temperature of the ceramics, which leads to an increase in the relative permittivity ε, piezoelectric modulus d_{31}, Young's modulus ^{p}Y, and the electromechanical coupling coefficient K_P of the samples. The improvement in these characteristics is due to an increase in the sintered ceramic density and a decrease in the porosity of the samples. Inhomogeneous sintering and the presence of pores in the samples lead to an increase in the dielectric loss tangent, which is especially noticeable in samples obtained by sonication with additional hydrostatic pressure. Under the influence of pressure, the number of powder particle collisions per unit time increases. This leads to an increase in the proportion of fine particles, a decrease in the average grain size, and a significant increase in the powder surface area. In this case, the sintering temperature of 1260 is low, and 1280 is high for obtaining a homogeneous dense sinter,

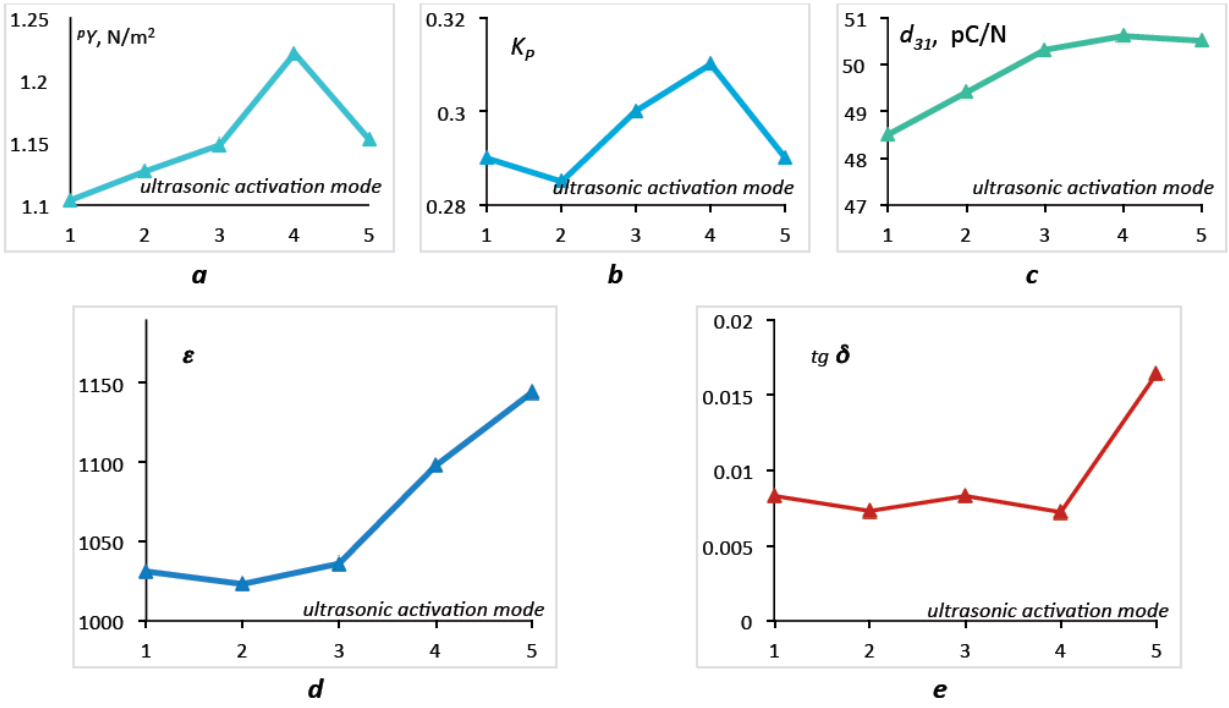

a – Young's modulus; ***b*** – electromechanical coupling coefficient; ***c*** – piezoelectric coefficient d_{31}; ***d*** relative permittivity**;** ***e*** – dielectric loss tangent.

Figure 5: Ceramic properties depending on ultrasonic activation mode.

which leads to the appearance of cracks and an increase in the dielectric loss tangent.

The surface morphology of ceramics obtained under various sonication modes is shown in Figure **6**.

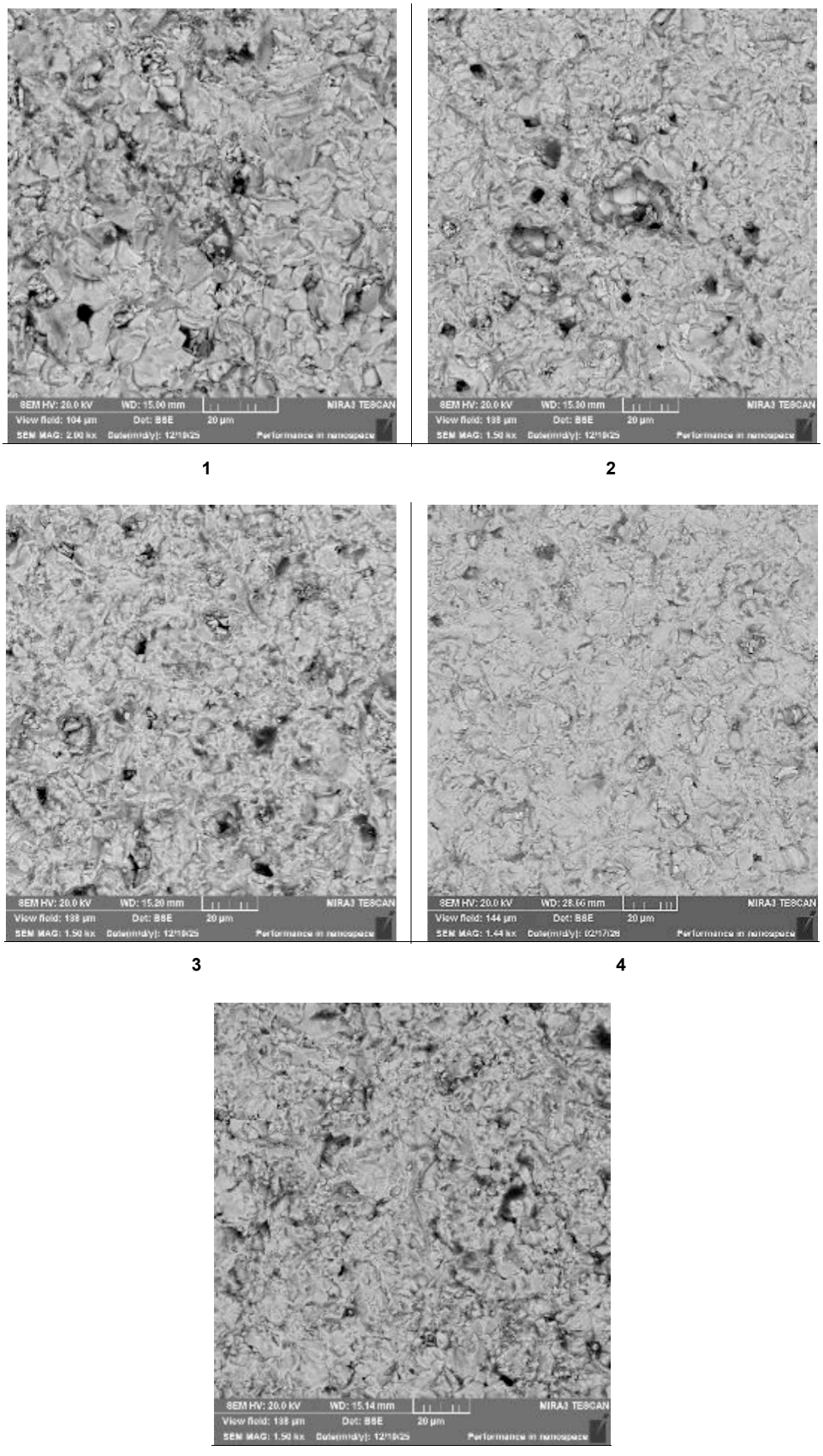

Figure 6: Surface morphology of ceramics obtained under various sonication modes with a resolution of 20 μm.

CONCLUSION

The SEM image shows that with increasing ultrasonic exposure duration, the pore size in the ceramic decrease, while the pore distribution within the composite and its composition become more uniform. Increasing the number of smaller grains in the batch significantly reduces the defectiveness of the ceramic microstructure due to improved powder flowability and, consequently, the quality of particle packing during pressing, which leads to an increase in the ceramic density. The addition of 0.2mol.% $NiFe_2O_4$ to 99.8mol.% (90 mol.% $BaTiO_3$ + 10 mol.% $CaTiO_3$), together with sonication of the batches before pressing, significantly reduces the sintering temperature of the samples (to 1300°C compared to 1400°C) and increases the permittivity by up to 3 times. Ceramics obtained after 90 min of sonication show the most homogeneous structure, which results in the best values of the relative permittivity ε, piezoelectric modulus d_{31}, Young's modulus ${}^{p}Y$, and electromechanical coupling coefficient K_P of the samples. The use of 30 minute sonication under excess hydrostatic pressure leads to a significant reduction in grain size in the batch, and the sintering temperature of 1280-1300°C proves excessive. The density of the ceramics increases, but cracks appear within the samples. This leads to a maximum increase in the relative permittivity and a proportional increase in the dielectric loss tangent, which does not allow for an increase in the electromechanical coupling coefficient and Young's modulus. The obtained result correlates with the data of studies [10, 11].

ACKNOWLEDGEMENTS

This research was supported by the Belarusian Academy of Sciences under SBFP 1.7 Research Project 4: "Development of New Functional Materials Based on Magnetoelectric Composites and Their Production Technologies." The authors thank Yu. Radyush for obtaining and discussing the X-ray diffraction analysis results.

AUTHOR'S CONTRIBUTION STATEMENT

N.N. Poddubnaya, V.V. Rubanik, and V.M. Laletin developed the original concept, planned the experiments, analyzed the results, and supervised all stages of this work.

V.M. Laletin, M.V. Kudybin, and P.A. Razbaev prepared the samples.

P.A. Razbaev, M.V. Kudybin, V.K. Frolov, and A.D. Shilin performed various stages of the presented experimental work and performed the calculations.

All authors discussed the results, provided critical comments, and contributed to the research, analysis, and preparation of the manuscript.

The X-ray diffraction analysis results were obtained and discussed with Yu. Radyush.

CONFLICTS OF INTEREST

The authors have no conflicts of interest.

REFERENCES

[1] Sayye SK. Study of structural phase transition and dielectric behavior of BiNaTiO3-SrTiO3 (BNT-ST) solid solution. Proceedings of the 14th Asian Conference on Solid State Ionics. 2014; 650-657. https://doi.org/10.3850/978-981-09-1137-9_114

[2] Zhenhua L, Wenwei G, Shaonan X, Xiaojuan L, Liang L, Qiang S, Qinhui Z. Bi2Ti2O7 modification-induced large strain characteristics in BNT-6BT piezoelectric ceramics. Appl. Phys. Lett. 2026; 128; 102902. https://doi.org/10.1063/5.0314093

[3] Sahoo AR, Reddy VR, Subohi O. (Ba, Sr)TiO3 (BST)-(Bi, Na)TiO3 (BNT) ceramics for energy storage and electrocaloric performance: optimization of BNT phase fraction. J. Mater Sci: Mater Electron. 2025; 36; 1597. https://doi.org/10.1007/s10854-025-15634-w

[4] Li D-X, Li Y, Shen Z-Y, Li Z, Wu J, Zhang Y. Bi(Ni1/2Hf1/2)O3-modified BNT-based ceramics for energy storage capacitors. J. Am. Ceram. Soc. 2026; 109:e70353. https://doi.org/10.1111/jace.70353

[5] Saeed H.M., AlShakarchi E. Preparation of new perovskite ferroelectric compound. Edelweiss Appl. Sci. and Technology. 2024; 8(6); 7022-7030. https://doi.org/10.55214/25768484.v8i6.3517

[6] Pittala S, Vishnunarayanan S, Anil Kumar PS. Magnetoelectric 0.2(CoFe2O4)-0.8(Ba0.85Ca0.15Zr0.1Ti 0.9O3) lead free composite for spintronic applications. IOP Conf. Series: Materials Science and Engineering. 2019; 577; 012062. https://doi.org/10.1088/1757-899X/577/1/012062

[7] Sasmal A, Maiti P, Chelvane JA, Arockiarajan A. Investigation of room temperature magnetoelectric coupling behaviour of novel lead-free (1-x)BaTi0.89Sn0.11O3-xCoFe1.9Bi0.1O3 particulate composites. Appl. Phys. A. 2024; 130; 265. https://doi.org/10.1007/s00339-024-07427-5

[8] Babu SN, Srinivas K, Bhimasankaram T. Studies on lead-free multiferroic magnetoelectric composites. J. Magn. Magn. Mater. 2009; 321(22); 3764-3770. https://doi.org/10.1016/j.jmmm.2009.07.029

[9] Lewin D, Shamsulbahrin S, Shvartsman VV, Lupascu DC. Stoichiometry of CoFe2O4 as a key to phase control and improved functional properties of multiferroic BaTiO3-CoFe2O4 bulk composites. Ceramics International. 2025; 51(18); Part A; 24596-24604. https://doi.org/10.1016/j.ceramint.2025.03.142

[10] Osoro GM, Bregiroux D, Thi MP, Levassort F. Structural and piezoelectric properties evolution induced by cobalt doping and cobalt/niobium co-doping in BaTiO3 Materials Letters. 2016; 166; 259-262. https://doi.org/10.1016/j.matlet.2015.12.086

[11] Liu W, Ren X. Large Piezoelectric Effect in Pb-Free Ceramics. Phys. Rev. Lett. 2009; 103; 257602. https://doi.org/10.1103/PhysRevLett.103.257602

[12] Khasanov OL, Dvilis ES, Polisadova VV, Zykova AP. Effects of powerful ultrasound exposure on the structure and properties of nanomaterials: a tutorial. Tomsk: Publishing house of Tomsk Polytechnic University. 2008; 28. [cited 2026]

[13] Laletin V, Kudybin M, Poddubnaya N, Filippov D. Magnetoelectric Properties of Lead-Free Three-Layer Structure Barium-Titanate-Piezoceramic Nickel. J. Compos. Sci. 2023; 7; 211. https://doi.org/10.3390/jcs7060211

[14] Sun Q., Gu Q., Zhu K., Jin R., Liu J., Wang J. Qiu J. Crystalline Structure, Defect Chemistry and Room Temperature Colossal Permittivity of Nd-doped Barium Titanate. SCiEntifiC Reports 2017; 7:42274. https://doi.org/10.1038/srep42274

[15] Ramoška T., Banys J., Sobiestianskas R., Petrović M.V., Bobić E., Stojanović B. Dielectric investigations of La-doped barium titanate. Processing and Application of Ceramics 2010; 4 (3); 193-198. https://doi.org/10.2298/PAC1003193R

[16] Xu C., Zhang Z., Zhangn J., Lei L., Zhang D., Fu Z. A new route to fabricate barium titanate with high permittivity. Ceramics International. 2012; 40; 10927-10931. https://doi.org/10.1016/j.ceramint.2014.03.090

[17] Pérez-Martín Y, Iglesias-Jaime AC, González-Abreu Y, Aday-Cantero AJ, Mariano MAS, Frolov VK, Shilin AD, Rubanik VV, Rubanik Jr. VV, Li Y, Yang T, Guerra JDS, Salak AN. Structure, morphology, ferroelectric and piezoelectric properties of (Bi0.5Na0.5)1-xBaxTiO3 ceramics produced with application of high-power ultrasound. J Electroceram. 2026. https://doi.org/10.1007/s10832-026-00493-6

[18] Mofa NN, Zhapekova AO, Sadykov BS, Bakkara AE, Sakhan MG, Bekentaeva AD, Mansurov ZA. Integrated use of mechanochemical and ultrasonic treatment to obtain highly dispersed silicon dioxide for special purposes. Combustion and plasma chemistry. 2019; 17; 123-132. Available from https://cpc-journal.kz/index.php/cpcj/article/view/168.

[19] Lian H, He Y, Liang X, Shi M, Liu L, Chen X. BN6BT ceramics via cold-sintering with annealing: Effects of grain size of precursor powders and annealing temperature. J Am Ceram Soc. 2024; 107:3194-3208. https://doi.org/10.1111/jace.19614

[20] Lee J. Influence of Particle Size on High-Temperature Sintering Behavior of Barium Titanate: Densification and Grain Growth. Journal of the American Ceramic Society. 2025; 109:e70378. https://doi.org/10.1111/jace.70378

https://doi.org/10.31875/2410-4701.2026.13.03